Check for
updates

Shallow-donor impurity effects on the far infrared electron–electron optical absorption coefficient in single and core/shell spherical quantum dots with Konwent-like confinement potential

E. B. Al[1] · E. Kasapoglu[1] · H. Sari[2] · I. Sökmen[3] · C. A. Duque[4]

© The Author(s), under exclusive licence to Springer Science+Business Media, LLC, part of Springer Nature 2022

Abstract

In this study, the electronic and optical properties of single or core/shell quantum dots, which are formed depending on the parameters in the selected Konwent potential, are investigated. Namely, the effects of the size and geometric shapes of quantum dots on the binding energy of the on-center donor impurity, the total absorption coefficient and refractive index which are including transitions between the some confined states, and the electromagnetically induced transparency between the lowest six confined states related to the donor impurity are investigated. We have used the diagonalization method by choosing a wave function based on the Bessel and Spherical Harmonics orthonormal function to find the eigenvalues and eigenfunctions of the electron confined within the quantum dots which have different types mentioned above. To calculate the optical absorption coefficients and electromagnetically induced transparency related to shallow-donor impurity, a two- and three-level approach in the density matrix expansion is used, respectively.

✉ E. Kasapoglu
  ekasap@cumhuriyet.edu.tr

✉ C. A. Duque
  carlos.duque1@udea.edu.co

1   Physics Department, Faculty of Science, Sivas Cumhuriyet University, 58140 Sivas, Turkey

2   Department of Mathematical and Natural Science Education, Faculty of Education, Sivas Cumhuriyet University, 58140 Sivas, Turkey

3   Dokuz Eylul University (retired), Izmir, Turkey

4   Grupo de Materia Condensada-UdeA, Facultad de Ciencias Exactas y Naturales, Instituto de Física, Universidad de Antioquia UdeA, Calle 70 No. 52-21, Medellín, Colombia

🖄 Springer

1 Introduction

Quantum dots (QDs) are one of the most important structures of low dimensional quantum systems which are used to manufacturing high-performance microelectronic and optoelectronic devices (Sugawara et al. 2005; McDonald et al. 2004; Böberl et al. 2008). Due to advances in material growth technologies such as molecular beam epitaxy and metal-organic chemical vapor deposition, the production of low-dimensional semiconductor systems which have varied shapes and sizes is became possible. The dependence of the electronic energy spectrum on the geometric shape of the confinement potential and size of QD is very strong. This dependency allows us to manipulate the electronic and hence, optical characteristics of QD. For this reason, QDs are very important topics for researchers both theoretically and experimentally. As well as the geometric form and size of the confinement potential of QDs (Niculescu et al. 2017; Talbi et al. 2021; El Aouami et al. 2020; El Haouari et al. 2017; Sharma et al. 2019; Tiutiunnyk et al. 2014), the externally applied electric, magnetic and intense laser fields (Sargsian et al. 2021; Rahimi et al. 2021; Al et al. 2021; Çakir et al. 2017; Holovatsky et al. 2017; Heyn and Duque 2020; Safarpour et al. 2015; Varshni 2001; Sari et al. 2020; Barseghyan et al. 2020) affect the electronic properties, which influences the optical properties of QD. In devices based on QDs, the effects caused by impurities are also quite important and thus there are a lot of researches involving impurity-related studies with a special focus on QDs (Laroze et al. 2016; Hayrapetyan et al. 2015; Sadeghi and Naghdi 2014; Karaca Boz et al. 2016; Rezaei and Kish 2013; Arif et al. 2021). In addition to the shape, size, and externally applied fields, the presence of impurities causes radical changes in the energy spectrum of the QDs and provides the desired optical transitions to be obtained with respect to the purpose. As known, controlled optical transitions are very important in the design of optoelectronic devices with tunable emission or transmission characteristics and ultra-narrow spectral line width.

The confinement of charge carriers in QDs causes to increase in the energy states, dipole matrix elements and the oscillator strength, which are related to a red or blue shift at absorption peak positions and an increase in peak amplitudes. Therefore, QDs are materials with great optical response (Vahdani 2014). This case prompted researchers to investigate optical phenomena such as optical absorption (Máthé et al. 2021; Al et al. 2021), optical rectification (Dahiya et al. 2020; Evangelou 2019; Makhlouf et al. 2021), second and third-order harmonic generations (Bahramiyan and Khordad 2014; Khordad and Bahramiyan 2014; Karabulut and Baskoutas 2009) and refractive index changes (Çakir et al. 2012; Zhang et al. 2010; Li et al. 2016). Optical absorption coefficients (OACs) of QDs which including impurity have different confinement potentials have been previously studied by many authors (Kria et al. 2020; Mora-Ramos et al. 2020; Kilic et al. 2020; Stevanović et al. 2019; Ghajarpour-Nobandegani and Karimi 2018; Shi and Yan 2017; Rahul et al. 2017; Khordad et al. 2016; Hosseinpour et al. 2016; Duque et al. 2016; Niculescu and Bejan 2015; Kasapoglu et al. 2014; Lu et al. 2011). Optical properties of QDs are investigated for: a cylindrical core-shell QD by Kria et al. (2020), the spherical sector-shaped QD by Mora-Ramos et al. (2020), a laser-driven two-dimensional disc-shaped QD by Kilic et al. (2020), a spherical QD by Stevanović et al. (2019), a typical ring-shaped elliptical QD by Ghajarpour-Nobandegani and Karimi (2018), core-shell ellipsoidal QDs by Shi and Yan (2017), a multilayer QD by Rahul et al. (2017), a lens-shaped QD with a finite confinement potential by Khordad et al. (2016), a parabolic QD by Hosseinpour et al. (2016), two QDs coupled

laterally with a circular cross-sectional shape by Duque et al. (2016), a pyramidal QD by Niculescu and Bejan (2015), a triangular two-dimensional QD by Kasapoglu et al. (2014), a QD with Woods–Saxon potential by Lu et al. (2011).

There are reports of important advances in the experimental development of QDs considering, for example, doping effects (Horiguchi et al. 1999; Erwin et al. 2005; Papagiorgis et al. 2016; Makkar and Viswanatha 2018; Zhang et al. 2019; Chang et al. 2020; Hartmann et al. 2000). The new growth techniques have been shown to open up a new generation of robust doped semiconductor QDs with cluster-free doping which will be suitable for various spin-based solid-state device technologies and overcome the longstanding challenges of controlled impurity doping.

In addition to the electronic structure in semiconductor nanostructures, optical absorption at inter-subband transitions, especially nonlinear absorption, is a very attractive subject. Electromagnetically induced transparency (EIT) has potential applications in many fields from nonlinear optics to quantum information science, namely nonlinear optics, optical memories, quantum optics, quantum computation, quantum information sciences and optical switches by controlling the light speed in low-dimensional semiconductors and researches about EIT continue intensively because of the potential applications mentioned above (Zhang et al. 2011; Fleischhauer et al. 2005; Marangos and Halfmann 2009; Beausoleil et al. 2004; Harris and Yamamoto 1998; Clarke et al. 2001; Ma et al. 2009). EIT which provides the coherent control of the optical properties of materials is one of the most interesting effects of quantum optics and it is a coherent optical nonlinearity that makes a medium transparent in a narrow spectral range around an absorption line. This transparency window leads to slow down and/or stop light that is one of the most striking EIT effects Hau et al. (1999). As known quantum confinement is mainly dealt with the energy of confined charge carriers (electrons and/or holes) in low dimensional systems. The energy levels of electrons in these systems are discrete, not continuum as in the bulk materials. QDs have perfect linear and nonlinear optical properties due to discrete energy levels which result from strong confinement that making them excellent for optoelectronic applications (Al-Khursan et al. 2009; Segal and Nitzan 2003; Atoyan et al. 2006; Crnjanski and Gvozdic 2004), and thus QDs are excellent structures for investigating the EIT Xu et al. (2006) and Chiam et al. (2009).

This study that we thought had not been studied before aims to examine the electronic and optical properties of $GaAs/Al_xGa_{1-x}As$ QDs with Konwent potential, which transform into single or core/shell QDs depending on the changes in the structure parameters. The organization of the paper is the following: Sect. 2 contains the presentation of the theoretical framework, in Sect. 3, we discuss the obtained results, and in Sect. 4 the conclusions are given.

2 Theory

2.1 Energies and wavefunctions

In this study we are interested in investigating the states of an electron-impurity system confined in a spherical GaAs/Al$_x$Ga$_{1-x}$As QD with confining potential described by the Konwent-like model. It is considered a shallow donor impurity located on the center of the structure and the effects of spatial variation of the effective mass are neglected. Once the wavefunctions and energies for the system have been obtained, without and with impurity,

we proceed to calculate, among others, the binding energy, the total absorption coefficient between the lowest three confined states, and the EIT between the lowest six confined states.

In the effective mass approach, the Hamiltonian for confined electron in KQD without impurity can be written as follows

$$H^{(0)} = \frac{\mathbf{p}^2}{2\,m^*} + V_{KP}(r),\tag{1}$$

where $\mathbf{p}$ and m^* are the momentum and the electron effective mass. $V_{KP}(r)$ is the confinement potential proposed by Konwent (1986) and defined as

$$V_{KP}(r) = V_0\Big[A\,\cosh\Big(\frac{r}{k}\Big) - 1\Big]^2,\tag{2}$$

where k is the parameter related to the dot-size in the radial direction, A is the structure parameter used to get different QD-shapes, and $V_0 = Q_c\,\Delta E_g$ is the potential depth. $Q_c = 0.6$ is the offset parameter of conduction band and $\Delta E_g = 1.247\,x$ eV (Adachi 1985) is the difference between the band gaps of $Al_xGa_{1-x}As$ and GaAs materials, where the aluminum concentration is taken as $x = 0.3$.

The r-dependence of the 3D-confinement potential in a GaAs-$Al_{0.3}Ga_{0.7}As$ KQD for five different values of the A-parameter is depicted in Fig. 1 (see Eq. (2)). As seen, the value of the A-parameter determines the shape of the potential. For $A < 1$, the system behaves as a core/shell QD where the potential height in the shell is regulated by the value of the A-parameter, reaching its maximum value when $A \to 0$. In the limit $A = 0$, $V_{KP}(r) = V_0$. As the A-parameter presents a finite value, but close to zero, the core/shell-like behavior appears with a core where the potential is constant and a shell whose distance from the QD-center systematically tends to infinity. As the A-parameter increases, approaching $A = 1$, a combination of two factors occurs: i) a systematic reduction of the potential barrier in the core region and ii) a systematic reduction of the core radius. The central barrier in the core disappears when $A = 1$ and its null value remains nearly constant over space up to a certain extent of the radial coordinate that depends on the value of the k-parameter, which controls the effective size of the QD. For $A > 1$ and k-decreasing, the system turns into a QD with parabolic potential in which it is possible to observe a shift of the potential bottom towards positive energies. It is important to highlight that the height of the central barrier in the core is definitely controlled by the A-parameter.

Fig. 1 (color online) The r-dependence of the 3D-confinement potential in a GaAs-$Al_{0.3}Ga_{0.7}As$ Konwent-like spherical quantum dot. Results are for five different values of the A-parameter with $k = 2.5$ nm and $V_0 = 0.225$ eV (see Eq. (2))
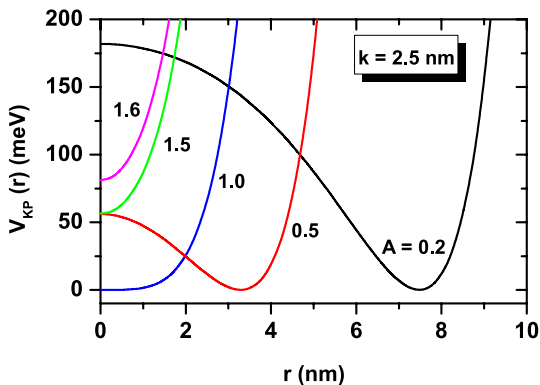
In the presence of central donor impurity, the Hamiltonian is written as

$$H = H^{(0)} - \frac{e^2 Z}{\varepsilon r}, \tag{3}$$

where $Z = 0$ ($Z = 1$) denotes the case without (with) the impurity, ε is the GaAs dielectric constant and r is the electron position. If the lengths are normalized to the effective Bohr radius $[a_B = \hbar^2 \varepsilon/(m^* e^2)]$ and the energies to the effective Rydberg $[R^* = \hbar^2/(2m^* a_B^2)]$, the dimensionless Hamiltonian is found as follows

$$H = -\nabla^2 + V_{KP}(r) - \frac{2Z}{r}, \tag{4}$$

where ∇^2 is the 3D-Laplace operator.

In order to find the energies and their corresponding wavefunctions, we have to solve the Schrödinger equation

$$H\psi_{nlm}(r, \theta, \phi) = E_{nlm}\psi_{nlm}(r, \theta, \phi), \tag{5}$$

where, n, l, and m are the principal, angular momentum, and magnetic momentum quantum numbers. To solve this equation, the Hamiltonian matrix is diagonalized by a series expansion using the electronic wavefunctions of the infinite spherical QD as the basis. This series expansion is given in the form (Holovatsky et al. 2017; Holovatsky et al. 2014; Holovatsky et al. 2018)

$$\psi_{nlm}(r, \theta, \phi) = \sum_j c_{n_j l_j} \psi_{n_j l_j m}^{(0)}(r, \theta, \phi), \tag{6}$$

where c_{nl} are the expansion coefficients and $\psi_{nlm}^{(0)}(r, \theta, \phi)$ is the total wavefunction describing the motion of the electron without impurity and it is expressed as follows in the form of product of the radial and angular functions by virtue of the QD symmetry

$$\psi_{nlm}^{(0)}(r, \theta, \phi) = \varphi_{nl}^{(0)}(r) Y_{lm}(\theta, \phi), \tag{7}$$

where $\varphi_{nl}^{(0)}(r)$ and $Y_{lm}(\theta, \phi)$ are the radial and spherical harmonics wavefunctions, respectively. $\varphi_{nl}^{(0)}(r)$ is defined in terms of the a-radius of the infinite spherical QD by the following equation

$$\varphi_{nl}^{(0)}(r) = \begin{cases} N j_l(k_{nl} r/a), & r < a \\ 0, & r \geq a. \end{cases} \tag{8}$$

Here N is a normalization constant and j_l are the spherical Bessel functions. Additionally, k_{nl} is the n-th zero of the j_l function. Note that due to the shape of the radial wave functions in Eq. (8), it is clear that in our model the Dirichlet boundary conditions are imposed on the surface of a sphere of radius a. In the present study, the a-radius value is chosen large enough so that at least over the first 20 energy states ascribed to the Konwent potential, the confinement effect associated with the sphere of radius a is less than 10^{-6} % of the reported energies. This condition is guaranteed by making $V_{KP}(a) = 10.0$ eV in Eq. (2). For example, for $k = 2.5$ nm and $A = 0.2$ the convergence of the first 20 confined states is guaranteed by making $a = 15$ nm while for $A = 1.6$ it is enough with $a = 6$ nm. In order that all the results can be compared with each other, we have decided to take a fixed value $a = 20$ nm. With respect to the number of terms in the sum appearing in Eq. (6), it is

important to clarify that the wave functions of the basis have been ordered guaranteeing an increasing order of the self-energies for an electron confined in a spherical QD with infinite confinement potential and radius a. The number of terms in the sum, that is $j = j_{max}$, has been chosen in such a way as to guarantee a convergence of the first 20 confined states of at least 10^{-4} meV. We have achieved this with $j_{max} = 320$ for those cases where the impurity is located in the center of the structure, a situation that preserves the spherical symmetry of the problem. By moving the impurity away from the QD center, a problem arises that preserves at least the azimuthal symmetry with respect to an axis passing through the center of the QD and the impurity position. In this case, to guarantee the convergence of the first 20 states, we have extended the sum up to $j_{max} = 620$.

It is important to note that in this work the Schrödinger equation corresponding to the Hamiltonian in Eq. (1) has also been numerically determined using the finite element method via the COMSOL-Multiphysics licensed software (2012a, b, c). In this case, given the azimuthal symmetry of the problem, whether in the case of an impurity in the center or outside the center of the QD, the problem has been expressed in cylindrical coordinates and an axis-symmetric model has been implemented to find the solution of the differential equation. For more details about the numerical method used, see for example Refs. Heyn et al. (2021), Pulgar-Velásquez et al. (2021). The finite element method parameters, particularly for this study, are: triangular mesh type, 5769 mesh vertices, 11278 triangles, 258 edge elements, 4 vertex elements, 0.5978 minimum element quality, 0.9231 average element quality, 0.2239 ratio element area, and 981.7 nm^2 for the mesh area.

The binding energy (E^b_{nlm}) is obtained from the difference between the energies in any nlm-states of the electron in the absence and presence of donor impurity and it is as defined by

$$E^b_{nlm} = E_{nlm}(Z = 0) - E_{nlm}(Z = 1), \tag{9}$$

where, $E_{nlm}(Z = 0)$ and $E_{nlm}(Z = 1)$ are the energies without and with impurity in the KQD, respectively.

We want to emphasize that in this study, we will focus our attention on states with $n = 1$ and $m = 0$. For the study of the OAC, we will use the first three states with $l = 0, 1, 2$. In the case of EIT, and due to the polarization of the two incident radiations, it will be necessary to extend the set to $l = 0, 1, 2, 3, 4, 5$.

In Figs. 2 and 3 we present the wavefunction projections in the $y = 0$ plane for a confined electron in a GaAs/Al$_{0.3}$Ga$_{0.7}$As KQD. In particular, Fig. 2 compares the ground state wavefunctions in the absence and presence of the on-center impurity for three values of the A-parameter and two values of the k-parameter. In Fig. 3 the ground state and the first two excited states wavefunctions in the presence of impurity are shown for the same combinations of the A- and k-parameters. Note that for $k = 2.5$ nm, we have used $a = 15$ nm while for $k = 5.0$ nm the corresponding value is $a = 25$ nm. This ensures that the effects of the infinite barrier in the outer region of the shell on the energies are minimal. In both cases, with and without impurity, the upper limit of the sum in Eq. (6) has been chosen to guarantee a convergence of 0.01 meV in the first ten energy levels. In Fig. 2, the spherical character imposed by the potential can be observed in all the presented wavefunctions. For $k = 5.0$ nm and $A = 0.2$, it is clearly appreciated that the maximum of the wavefunction is located in the shell region and that the presence of the impurity generates an increase in the density of probability in the central region of the structure; this despite the presence of the potential barrier present in the core region. In the case of $k = 2.5$ nm and $A = 0.2$ the core/shell character is not very clear because a large part of the electronic wavefunction is
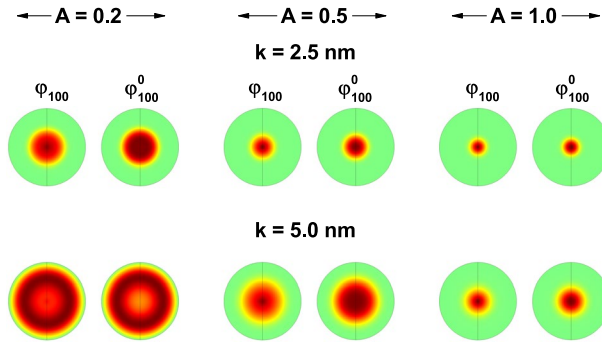
Fig. 2 (color online) The $y = 0$ projection of the ground state correlated (φ_{100}) and uncorrelated (φ_{100}^0) electron wave function in the GaAs/Al$_{0.3}$Ga$_{0.7}$As Konwent-like spherical quantum dot. Results are for three values of the A-parameter with $k = 2.5$ nm and $k = 5.0$ nm. In the case of the correlated wave function, the shallow-donor impurity is localized at the center of the dot. The colors-code is as follows: maximum and positive wave function (red) and zero wave function (green)
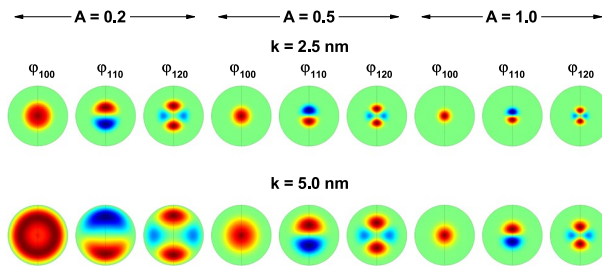

Fig. 3 (color online) The $y = 0$ projection of the correlated electron wave function for the ground state (φ_{100}) and the two first excited states ((φ_{110}) and (φ_{120})) in a GaAs/Al$_{0.3}$Ga$_{0.7}$As Konwent-like spherical quantum dot. Results are for three values of the A-parameter with $k = 2.5$ nm and $k = 5.0$ nm. The shallow-donor impurity is localized at the center of the dot. The colors-code is as follows: maximum and positive wave function (red), maximum and negative wave function (blue) and zero wave function (green)

located in the core region; this gives the little spatial extension of the structure. Consistent with the attractive potential associated with the impurity, in the all cases of Fig. 2, a reduction in the spatial extension of the wavefunctions is observed, compared to the case without impurity.

In Fig. 3, where the ground state and the first two excited states are presented, in the presence of impurity, the following characteristics are observed: (i) as mentioned above, the ground state has spherical symmetry, that is, it corresponds to s-like states, where the wavefunctions are more spread out in space as k-increases and A-decreases, (ii) in all considered cases of A- and k-parameters, the first excited state has p_z-like symmetry, corresponding to two antinodes located symmetrically on the z-axis and having the opposite sign; in this case the wave function is null at $r = 0$ (or $z = 0$), and (ii) the second excited state has d-like symmetry with two antinodes of the same sign located symmetrically on the z-axis and a thorus region of maximum amplitude, but opposite sign, which has axial symmetry with respect to the z-axis. Compared to the ground state, the first and second excited states have a greater spatial extension, and this extension increases with the

increase (decrease) of the k-parameter (A-parameter). Considering z-polarized resonant incident radiation, and taking into account the symmetries of the wave functions, clearly the $\psi_{100} \rightarrow \psi_{110}$ and $\psi_{110} \rightarrow \psi_{120}$ transitions are allowed while the $\psi_{100} \rightarrow \psi_{120}$ transition is forbidden.

2.2 Optical absorption coefficient

Photoabsorption is the phenomenon of transition from low energy level to high energy level by absorption of a photon in any quantum system. When a photon with energy $\hbar \omega \geq E_j - E_i$ is absorbed, a transition takes place between levels with energy E_i and E_j. The linear, third-order nonlinear, and total optical absorption coefficient (OAC) corresponding to these transitions are described as follows, respectively:

$$\alpha^{(1)}(\omega) = \sqrt{\frac{\mu}{\varepsilon_r}} \frac{\sigma_s \, \hbar \, \omega \, |M_{ij}|^2 \, \Gamma_{ij}}{(E_{ij} - \hbar \, \omega)^2 + (\hbar \, \Gamma_{ij})^2} \, , \tag{10}$$

$$\alpha^{(3)}(\omega, I) = -\sqrt{\frac{\mu}{\varepsilon_r}} \left(\frac{I}{2 \, n_r \, \varepsilon_0 \, c} \right) \frac{\sigma_s \, \Gamma_{ij} \, \hbar \, \omega \, |M_{ij}|^2}{[(E_{ij} - \hbar \, \omega)^2 + (\hbar \, \Gamma_{ij})^2]^2}$$
$$\left[4 \, |M_{ij}|^2 - \frac{|M_{jj} - M_{ii}|^2 \, [3 \, E_{ij}^2 - 4 \, E_{ij} \, \hbar \, \omega + \hbar^2 \, (\omega^2 - \Gamma_{ij}^2)]}{E_{ij}^2 + (\hbar \, \Gamma_{ij})^2} \right] , \tag{11}$$

and

$$\alpha(\omega, I) = \alpha^{(1)}(\omega) + \alpha^{(3)}(\omega, I), \tag{12}$$

where ω is the angular frequency of the incident photon, μ is the vacuum magnetic permeability, ε_r is the real part of the GaAs susceptibility, σ_s is the electron density, $\Gamma_{ij} = 1/T_{ij}$ (where T_{ij} is the relaxation time) is the non-diagonal matrix element known as the relaxation rate of the final and initial states, $E_{ij} = E_j - E_i$ is the transition energy between the initial and final states, $I = 2 \, \varepsilon_0 \, n_r \, c \, |\tilde{E}|^2$ (where $|\tilde{E}|$ is amplitude) is the intensity of the incident resonant field, n_r is the GaAs refraction index, c is the vacuum light speed, and $\varepsilon_0 = 8.85 \times 10^{-12}$ F/m is the vacuum permittivity. M_{ij} is the dipole transition matrix element, and for incident resonant radiation polarized in the z-direction it is given as

$$M_{ij} = \langle \psi_i | e \, r \, \cos \theta | \psi_j \rangle, \tag{13}$$

where ψ_i and ψ_j are the wavefunctions representing the initial and final states, respectively.

In accordance with the energy conservation law, every probable transition in the absorption spectrum can not be observed. In addition to the energy conservation, the angular momentum conservation and several symmetry rules have to also be provided. All permitted transitions are added in the dipole transition elements, and the cases where the dipole transition element is nonzero are sought. So, for a linearly polarized light interacting with the electric field polarized in the z-direction, only the z-component of the dipole transition element is nonzero, while the other components are zero. According to the property of spherical harmonics, only dipole transitions are allowed between cases that supply the rule $\Delta l = \pm 1$. Also $M_{jj} - M_{ii}$ is zero for the donor impurity at the center of QD. The resonance conditions are $\hbar \omega_1 = \sqrt{E_{ij}^2 + (\hbar \Gamma_{ij})^2}$ and

$\hbar\,\omega_3 = \frac{1}{3}\left(E_{ij} + \sqrt{4\,E_{ij}^2 + 3\,(\hbar\,\Gamma_{ij})^2}\right)$ for linear and third-order nonlinear OACs, respectively. We define the following two-functions which are associated to the resonant conditions

$$\Omega = e^{-2}\sqrt{E_{ij}^2 + (\hbar\,\Gamma_{ij})^2}\;|M_{ij}|^2 \tag{14}$$

and

$$\Gamma = \frac{e^{-4}}{3}\left(E_{ij} + \sqrt{4\,E_{ij}^2 + 3\,(\hbar\,\Gamma_{ij})^2}\right)|M_{ij}|^4 . \tag{15}$$

2.3 Electromagnetically induced transparency

In Fig. 4 we present the three energy level system in the Λ-configuration to study the impurity related EIT in KQD. The interlevel transition between the $|a\rangle$ and $|c\rangle$ ($|b\rangle$ and $|c\rangle$) states is dipolarly allowed through the probe (control) field while the transition between the $|a\rangle$ and $|b\rangle$ states is dipolarly prohibited ($M_{ac} \neq 0$, $M_{bc} \neq 0$, and $M_{ab} = 0$). The parameters ω_p and $\mathbf{E_p}$ (ω_c and $\mathbf{E_c}$) are the frequency and strength of the probe (control) field. The probe and control lasers are detuned from the resonance frequencies by $\Delta_p = \omega_{ca} - \omega_p$ and $\Delta_c = \omega_{cb} - \omega_c$.

By using the rotating-wave approximation, the OAC ($\alpha(\omega)$) and refraction index (n_T, RI) for a three-level system in the Λ-configuration interacting with two applied laser pulses (probe and control) are, respectively

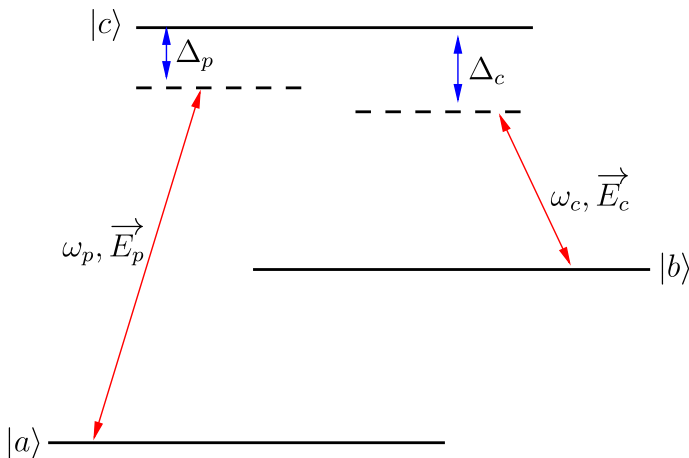$$\alpha(\omega) = \frac{\omega\,\Im(\chi)}{c\,n_T} \tag{16}$$

and

Fig. 4 (color online) The three-energy levels in the Λ-configuration for the electromagnetically induced transparency occurrence

$$n_T = \sqrt{\frac{n_r^2 + \Re(\chi) + \sqrt{(n_r^2 + \Re(\chi))^2 + \Im(\chi)^2}}{2}} \tag{17}$$

where

$$\Im(\chi) = \frac{\sigma_s M_{ca}^2}{\varepsilon_0 \hbar} \frac{\gamma_{ca} \left[\gamma_{ba}^2 + (\Delta_p - \Delta_c)^2 \right] + \gamma_{ba} \Omega_c^2}{\Theta} \tag{18}$$

$$\Re(\chi) = \frac{\sigma_s M_{ca}^2}{\varepsilon_0 \hbar} \frac{(\Delta_p - \Delta_c) \left[(\Delta_p - \Delta_c) \Delta_p - \Omega_c^2 \right] + \Delta_p \gamma_{ba}^2}{\Theta} \tag{19}$$

and

$$\Theta = \left[\Omega_c^2 + \gamma_{ca} \gamma_{ba} - \Delta_p(\Delta_p - \Delta_c) \right]^2 + \left[\Delta_p \gamma_{ba} + (\Delta_p - \Delta_c) \gamma_{ca} \right]^2. \tag{20}$$

Here $\Omega_c = \mathbf{M_{ca}} \cdot \mathbf{E_p}/(2\hbar)$ is the half of the Rabi frequency and γ_{ij} is the decay rate between the i and j states composed from the radiative decay rate due to the spontaneous emission and the dephasing rate. For details, see Ref. Bejan (2017).

3 Results and discussion

In this section, the effects of potential parameters on the binding energies, OACs, and EIT in the GaAs/Al$_{0.3}$Ga$_{0.7}$As Konwent-like spherical QD is analyzed. The physical parameters used in our calculations are: $\varepsilon = 13.18$, $V_0 = 0.225$ eV, $m^* = 0.067\,m_0$ (where m_0 is the free electron mass), $T_{ij} = 1.0$ ps, $\mu = 4\pi \times 10^{-7}$ H/m, $n_r = 3.63$, $\sigma_s = 3.0 \times 10^{23}$ m^{-3}, and $I = 100$ MW/m^2 (Al et al. 2021). Other parameters are: $\Omega_c = 40$ THz, $\gamma_{ba} = 0.1$ THz, and $\gamma_{ca} = 5$ Thz (Bejan 2017).

The Fig. 5 shows the changes of energy without impurity ($Z = 0$) and with impurity ($Z = 1$) and binding energy as a function of the A-parameter for two different k-values in a KQD. Since the electron confinement increases due to the transformation of the structure from core/shell KQD towards a single KQD with increasing the A-parameter, the uncorrelated and correlated energies are increasing functions of the A-parameter. Furthermore, all energies mentioned above decreases with the k-parameter since the electron confinement decreases. Furthermore, with the addition of impurity to the structure, the negative Coulomb potential between the electron and the impurity causes a reduction in energy. Finally, it is seen that the impurity-free and impurity-containing energies increase gradually towards the higher states ($E_{100} < E_{110} < E_{120}$). We can see that the effect of impurity is systematically reduced as one passes from the ground state to the first excited state and subsequently to the second excited state. It is clear that the excited states are more extended in space and thus the interaction with the impurity becomes weaker. This explains the reason why for the binding energy of the three states shown, $E_{100}^B > E_{110}^B > E_{120}^B$ is satisfied. Note the trend exhibited by the binding energy for the three states shown. They are increasing functions of the A-parameter. However, it can be seen that for large values of A-parameter there is a tendency to reach constant values. This is explained by the fact that for a sufficiently large A value, the system has the tendency to reach the limit of a strongly

Fig. 5 (color online) The first three uncorrelated ($Z = 0$, solid lines) and correlated ($Z = 1$, dashed lines) confined energy levels in the GaAs/Al$_{0.3}$Ga$_{0.7}$As Konwent-like spherical quantum dot as a function of the A-parameter. The results are for $k = 2.5$ nm (a) and $k = 5.0$ nm (b) with the on-center shallow-donor impurity. The inset in each panel shows the corresponding binding energies obtained through the difference $E_{1j0}^0 - E_{1j0}$ with $j = 0, 1, 2$
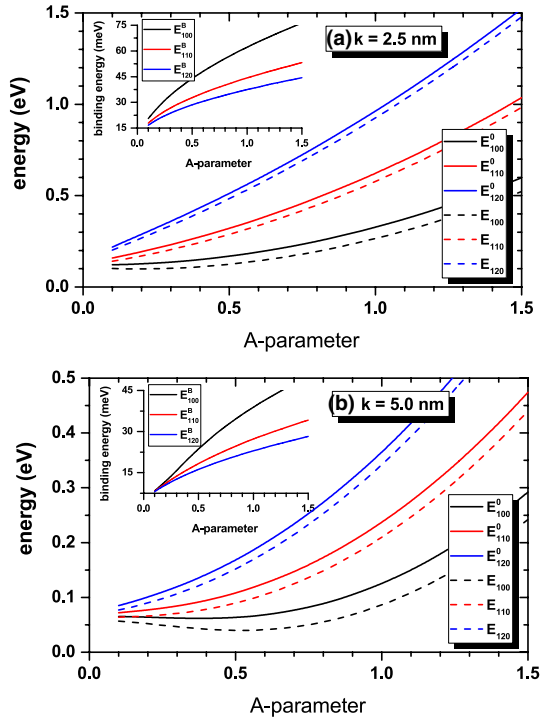
confined zero-dimensional hydrogen system. The binding energy grows as A-increases due to the fact that the infinite potential barrier, located on the outside of the KQD, approaches towards the central region of the structure, pushing the electronic wavefunction towards the impurity position. With this, there is

a reduction in the average electron-impurity distance, which leads to a gradual increase in the Coulomb interaction and consequently to an increase in the binding energy.

The energy transitions (a1, a2), the reduced dipole matrix elements (b1, b2), the Ω-function (c1, c2, see Eq. (14)), and the Γ-function (d1, d2, see Eq. (15)) in the GaAs/Al$_{0.3}$Ga$_{0.7}$As Konwent-like spherical QD as a function of the A-parameter are depicted in Fig. 6. The results are for $k = 2.5$ nm (upper row) and $k = 5.0$ nm (lower row) with on-center shallow-donor. Solid lines are considering transitions from the ground state to the first excited state ($\psi_{100} \to \psi_{110}$) whereas dashed lines are considering transitions from the first excited state to the second excited state ($\psi_{110} \to \psi_{120}$). From Fig. 4a1, a2, it is observed that all the transition energies are increasing functions of the A-parameter. This is in perfect agreement with the fact that as the confinement of the carriers increases due to the effective reduction in the KQD-size, the separation between the energy levels also increases, as can be seen in Fig. 6, and hence the consequent increase of transition energies. It is clear that $\Delta E_{12} > \Delta E_{12}^0$ because the presence of the impurity affects mainly the ground state with a reduction in energy. Comparing the first and second excited states, the impurity produces a more noticeable effect on the first one, hence the reason why $\Delta E_{23} > \Delta E_{23}^0$ is explained. Comparing Fig. 6a1 and a2, it can be seen in the first case that the calculated variation of the A-parameter generates a change in the transition energy of 0.5 eV while in the second one the variation is of the order of 0.2 eV. The larger the structure, the closer the energy states and the smaller the transition energy. Taking into account that the increase in the
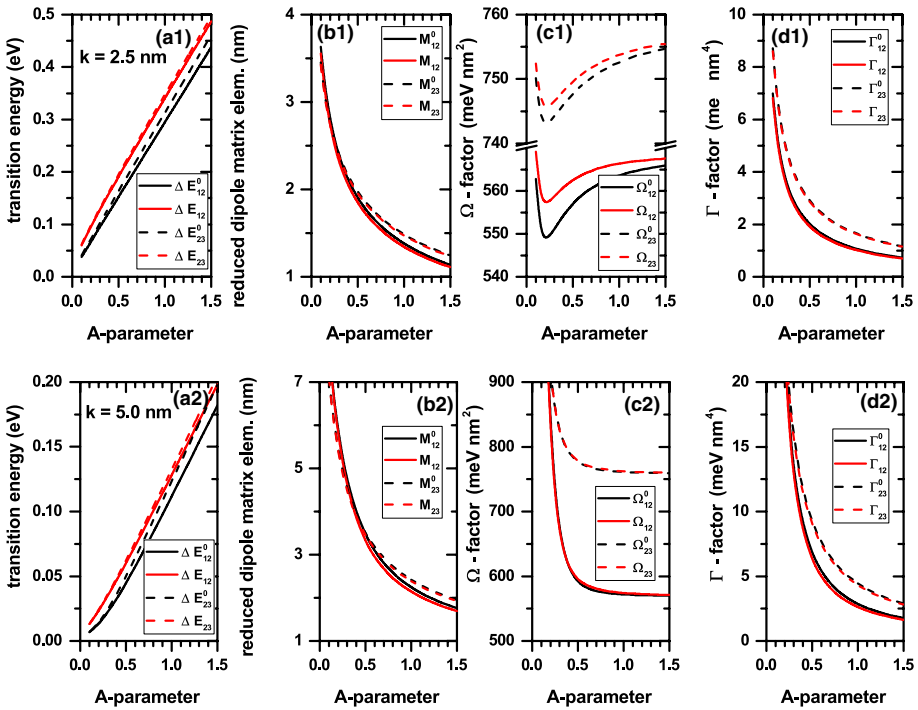
Fig. 6 (color online) Energy transitions (a1, a2), reduced dipole matrix elements (b1, b2), Ω-function (c1, c2), and Γ-function (d1, d2) in the GaAs/Al$_{0.3}$Ga$_{0.7}$As KQD as a function of the A-parameter. The results are for $k = 2.5$ nm (a1, b1, c1, d1) and $k = 5.0$ nm (a2, b2, c2, d2) with the shallow-donor impurity localized at the center of the dot. Solid lines are considering transitions from the ground state to the first excited state $(1 \rightarrow 2)$ whereas dashed lines are considering transitions from the first excited state to the second excited state $(2 \rightarrow 3)$

A-parameter translates into an effective decrease in the KQD-size, this explains the reason why in panels 6b1, b2 the reduced dipole matrix element is always a decreasing function of the A-parameter. The larger the original structure (which corresponds to the one whose k-parameter is the largest), the more noticeable is the variation of M_{ij}^0 and M_{ij}. While in Fig. 6b1 the variation exhibited by the matrix elements is of the order of 2.5 nm, in Fig. 6b2 the changes exceed 5.0 nm. In the calculation of the Ω- and Γ-functions, according to Eqs. (14) and (15), it is evident that these are dominated by the behavior of the dipole matrix elements. Then, Fig. 6d1 is in line with the decreasing behavior of the curves in Fig. 6b1. The same can be seen in Fig. 6c2 and d2 with respect to that shown in Fig. 6b2. However, the behavior of Fig. 6c1 shows that the Ω-function comes from a competitive effect between the transition energy, which is always increasing with the A-parameter, and the dipole matrix elements, that are always a decreasing functions of the A-parameter. However, note that in Fig. 6c1 the changes of the Ω-function in the entire range of the A-parameter do not exceed 20 meV nm^2.

In Fig. 7 the total OAC is presented as a function of the incident photon energy in the presence of the impurity atom for $k = 2.5$ nm (a) and $k = 5.0$ nm (b) and several A-values. Here, since the third order nonlinear OAC is very small (due to the relatively low value of the resonant radiation intensity that we have used to generate the optical absorption,
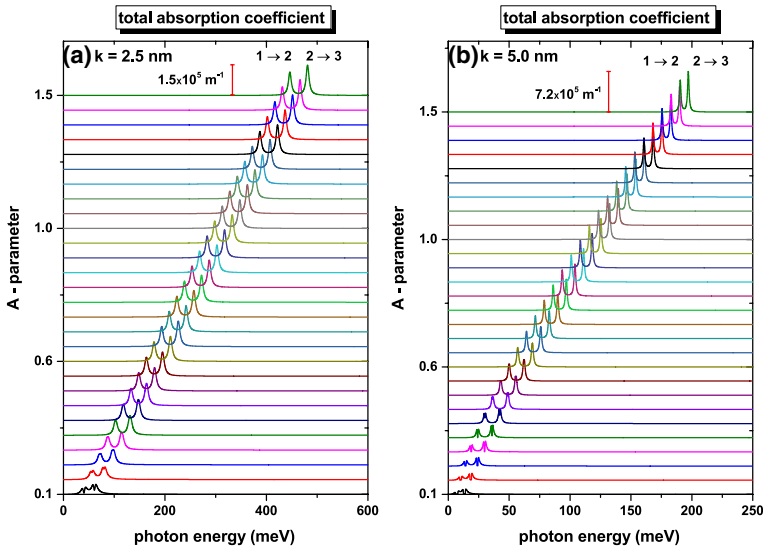
Fig. 7 (color online) The shallow-donor impurity related total optical absorption coefficient in the GaAs/ $Al_{0.3}Ga_{0.7}As$ KQD as a function of the incident photon energy for several values of the A-parameter. The results are for $k = 2.5$ nm (a) and $k = 5.0$ nm (b) with the shallow-donor impurity localized at the center of the dot. Calculations are considering the $1 \rightarrow 2 = \psi_{100} \rightarrow \psi_{110}$ and $2 \rightarrow 3 = \psi_{110} \rightarrow \psi_{120}$ transitions

$I = 100$ MW/m^2), the total OAC gives an equivalent result with the linear one, so we prefer to show only the total OAC. However, from Eqs. (10) and (11), it is observed that for high intensities of the incident radiation it is possible that the third order correction in the absorption coefficient, which depends on the intensity, becomes of the same order of magnitude as the first order correction. In this case an absorption cancellation effect may even appear, a situation known as bleaching of the optical absorption coefficient. In such situations, clearly instead of discussing the total OAC, it is better to present the separate analysis of each of the corrections that make it up. In Fig. 7a, the effect of the third-order correction is only noticeable in the first curve for $A = 0.1$, while in Fig. 7b, it can be seen that the third-order correction order is relevant for $A < 0.3$. The peak positions of the total OACs for the transitions corresponding to the case with impurities shift to the blue with the increase of A-parameter. Since the energy difference between the levels of interest increases with the A-parameter, the peak positions of the total OAC shift to blue. We also see that while the peak amplitude of the total OAC is almost constant for single KQD ($A > 1$), it decreases for the core/shell KQD ($A = 0.1$). This is a result related to the Ω-factor given in Fig. 6c1, c2, where the resonant peak of linear OAC is directly proportional to the Ω-factor (see Eqs. (10) and (14)). Although the wavefunctions overlap better in the core/shell structure (see Figs. 2 and 3), the Ω-factor decreases due to the decrease in the transition energy. According with the results in Fig. 6, the presence and absence of the impurity does not create a noticeable change in absorption amplitudes. However, the presence of impurity causes an increase in transition energies as seen in Fig. 6a1, a2, and thus the peak positions of the total OAC shift to the blue. Finally, it should be noted that the peak positions of the total OAC associated with the $\psi_{110} \rightarrow \psi_{120}$ transition always occur at higher energies than those associated with the $\psi_{100} \rightarrow \psi_{110}$ transition. Because, as seen in Figs 6a1, a2, ΔE_{23} transition energy is greater than ΔE_{12} transition energy for all

parameter values. At the same time, the peak amplitudes of the total OAC corresponding to the $\psi_{110} \rightarrow \psi_{120}$ transitions are always greater than those of the $\psi_{100} \rightarrow \psi_{110}$ transitions. As a result of the better overlap of the wave function of the ψ_{110} state with the wave function of the ψ_{120} state, the Ω-factor is larger for the $\psi_{110} \rightarrow \psi_{120}$ transition (see Fig. 6c1, c2).

At this point it is important to establish some aspects related to the degree of validity of the results shown in Fig. 7. Note that, in both cases, Fig. 7a and b, the transitions all fall in the infrared region, that is, with energies in the range 1.24 meV to 1700 meV. In the case of Fig. 7b, they are transitions in the far infrared region while in Fig. 7a, for sufficiently high values of the A-parameter ($A > 1$), there is a significant shift towards the mid infrared region. From the results in Fig. 1, for the case $k = 2.5$ nm, which corresponds to the results in Fig. 7a, it can be seen that for $A \geq 1$, the system is that of a strongly confined single QD. The potential approaches infinity for $r < 4\,nm = 0.38\,a_B$, where $1\,a_B = 10.4$ nm is the GaAs effective Bohr radius (see the first paragraph of this section for the effective mass and dielectric constant parameters used in this study). In the regime of $A \geq 1$, due to the infinite potential barrier on the exposed frontier of the QD, the system is simulating a GaAs/vacuum QD, that is, a GaAs QD with surface exposed to vacuum, which behaves as a infinite potential barrier. This type of structures can be obtained experimentally by the droplet epitaxy technique with exposed surfaces (Heyn et al. 2017; Elborg et al. 2017; Mora-Ramos et al. 2021). In the case of $A < 1$, it is observed that for $k = 2.5$ nm, for example, the transition energies generally exceed the height of the central barrier. This is an indication that for this range of A-parameters, where the system simulates core/shell QDs with exposed outer surface given the infinite potential barrier, there is still a high degree of confinement on the carriers. We emphasize that in general, in the range of the A-parameters considered in Fig. 7a and b, the sizes of the single and core/shell QDs are less than $1\,a_B/2\,a_B$ with infinite confinement potential on the surface. This high confinement effect becomes much more visible as excited states are considered for electron-electron transitions both in the absence and in the presence of donor impurities.

We have to stress that the absorption coefficient corresponds to a collective response. In a macroscopic medium, the individual dipole moments respond to the presence of an electric field, of light in that case. When the treatment of the absorption coefficient is done, this is a statistical treatment, that is, from the statistical operator the trace of the operator is calculated and the average is obtained. Therefore, in an analogous way, it is possible to think that, in a QD, regardless of whether there is only one QD and whether it is a nanoscopic structure, there is a density of electrons. In the QD problem, there is not a single electron, in a QD there is a collectivity of electrons that is given by an electron density. In a real sample of QDs it is possible to think about a density of QDs in a matrix. Inside a single isolated QD, is possible to talk about a density of electrons, and in that case, that number is the one that acts as if it were a density of many particles that are responding to the electromagnetic interaction. Therefore, actually, given the reduced size of the QD, there is an electron density, and that is what is normally the macroscopic quantity that acts as a coefficient to give the absorption of the system, in analogy to what a macroscopic system is.

Next, we turn our attention to the impurity-related EIT in a GaAs/Al$_{0.3}$Ga$_{0.7}$As KQD. We have chosen a QD with $k = 5.0$ nm and considering on-center impurity. Our results are presented as a function of the A-parameter and probe field energy.

In Fig. 8a, the energies of the six lowest states are presented as a function of the A-parameter. In the inset of Fig. 8a, we report the transition energy between the ground state and the 5th excited state (E_{61}). In Fig. 8b our results for the reduced dipole matrix element are depicted for the $1 \rightarrow 6$, $3 \rightarrow 6$, and $1 \rightarrow 6$ transitions considering z-polarized probe and control incident fields. Consistent with what has already been explained above,

Fig. 8 (color online) **a** The first six correlated confined energy levels in the GaAs/Al$_{0.3}$Ga$_{0.7}$As KQD as a function of the A-parameter. The results are for $k = 5.0$ nm with the shallow-donor impurity localized at the center of the dot. The inset shows the $1 \rightarrow 6$ transition energy. The probe field is associated to the $1 \rightarrow 6$ transition whereas the control field is associated to the $3 \rightarrow 6$ transition. In **b** the reduced dipole matrix elements for the $1 \rightarrow 6$, $1 \rightarrow 3$, and $3 \rightarrow 6$ transitions are presented. Note that $M_{13} = 0$
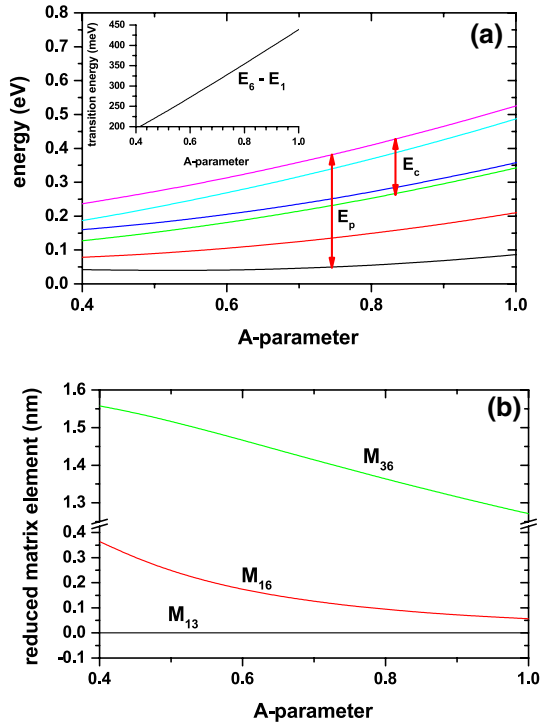
the increasing character of the energies for the all states shown in Fig. 8a corresponds to an increase in the confinement of the charge carriers as the effective size of the heterostructure decreases due to the increase of the A-parameter. In what follows, for convenience, the wavefunctions and energies of the confined states will be identified simply as ψ_1, ψ_2, ψ_3, ... and E_1, E_2, E_3, ... The higher the energy of a state, the more extended in space is its wavefunction, which has the consequence that the growth rate with the A-parameter is higher for the ψ_6 state than for the ψ_1 state. This has the final effect that the transition energy E_{61} grows linearly with the A-parameter, as shown by the inset in Fig. 8a. The reduction of the spatial extent of the structure as the A-parameter increases explains why the reduced dipole matrix elements in Fig. 8b decrease as the A-parameter increases. Again, the more extended the wave functions are in space, the more sensitive is the variation of the reduced dipole matrix element to changes in the A-value, a situation that is evident when comparing M_{36} and M_{16}. It is clear that $M_{13} = 0$ because the wavefunctions of the ψ_1 and ψ_3 states have the same symmetry.

In Fig. 9a and b, our results for the on-center shallow-donor impurity related total OAC and RI in the KQD (with $k = 5.0$ nm) are presented as a function of the incident probe photon energy for several values of the A-parameter taking into account the ψ_1, ψ_3, and ψ_6 states in the three-levels Λ configuration. Dashed lines are for $\Omega_c = 0$, in which case the OAC presents only one resonant structure located at $E_p \sim E_{61} = E_6 - E_1$ (where E_p is the incident probe photon energy). The position of the resonant peak shows a blueshift as the A-strength increases in complete agreement with the dependence shown with said parameter on the transition energy reported in the inset of Fig. 8a. The
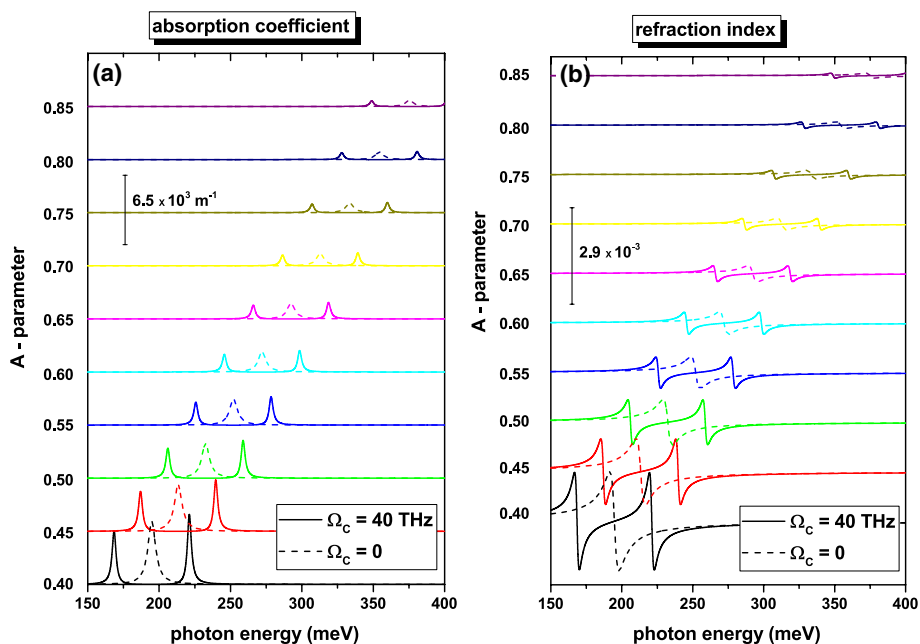
Fig. 9 (color online) The shallow-donor impurity related total optical absorption coefficient **a** and refraction index **b** in the GaAs/Al$_{0.3}$Ga$_{0.7}$As KQD as a function of the incident probe photon energy for several values of the A-parameter. The results are for $k = 5.0$ nm with the shallow-donor impurity localized at the center of the dot. Calculations are considering the $1 \rightarrow 6$ transition excited by the probe laser, whereas the control field involves the $3 \rightarrow 6$ transition. Dashed lines are for $\Omega_c = 0$, whereas solid lines are for $\Omega_c = 40$ THz (in this case, the non-zero control field activates the electromagnetically induced transparency). Additionally, in these figures, $\Delta c = 0$

systematic fall of M_{16} in Fig. 8b, explains the reason why there is an attenuation of the magnitude of the resonant peaks in Fig. 9a as A-increases. Consistent with only a resonant structure for the OAC when $\Omega_c = 0$, the results presented in Fig. 9b for the RI show that it becomes null at $E_p = E_{61}$ and that concerning this energy value, the RI shows two resonant structures that have inversion symmetry. For $\Omega_c = 0$ and taking a constant value of the A-parameter, the magnitudes of the resonant structures in the OAC and RI are controlled by the γ_{61}-parameter. When $\Omega_c \neq 0$, the control field is activated, and at that moment, the EIT effect appears. Precisely at the same value where the OAC presented the maximum when $\Omega_c = 0$, in the case of a finite Ω_c value, the OAC is now suppressed, and it is replaced by two resonant structures symmetrically located concerning zero absorption and whose separation is controlled by the Ω_c magnitude. The magnitude of these structures is not the same, the resonant peak located at higher energy is higher. This is associated with the linear term with the probe photon energy that controls the OAC. When the EIT is activated, two resonant structures appear in the OAC, in the same position as these, the RI replicates the results presented with $\Omega_c = 0$. In each resonant peak of the OAC, the RI becomes null with two structures that satisfy the inversion symmetry. It is important to note that for the case $\Omega_c \neq 0$, the magnitude of the resonant structures in the OAC and RI is controlled simultaneously by the γ_{61} and γ_{31} parameters,

with the dominant effect associated with γ_{31}. For a high enough value of γ_{31}, the RI can go from four to just two resonant structures.

4 Conclusions

In this study, the electronic and optical properties of GaAs/Al$_{0.3}$Ga$_{0.7}$As QD with Konwent potential, which transform into single or core/shell QDs depending on the changes in the structure parameters are investigated. Our results include: *i*) Uncorrelated ($Z = 0$) and correlated ($Z = 1$) energies of the electron as the functions of the shape (*A*-parameter) and size (*k*-parameter) of KQDs, *ii*) the binding energies for shallow donor impurity located on the center of the QDs, *iii*) the total OACs for the allowed transitions between the lowest three confined states, and *iv*) the impurity-related EIT between the lowest six confined states, respectively. Due to the strong quantum confinement caused by the change in the structure parameter in the potential, that is, the changes in size and geometric shape, it is seen that the QDs under investigation have a significant effect on the energy and optical spectrum. Moreover, it is seen that with selected realistic confinement potential and a special selection of the structure parameters, the optical response of the system can be tailored in a controllable manner. In this context, the results obtained indicate that QDs are highly important structures for optoelectronic applications.

About the degree of applicability of the results presented in this study, it is important to say that, in fact, in the case of single QDs, when in our model $A \geq 1$, we are in the range of spherical QDs with infinite confinement potential at the surface. This in reality corresponds to QDs with exposed surface; for example, GaAs QDs surrounded by a vacuum. Another example corresponds to the well-known colloidal QDs made of a relatively small bandgap semiconductor that are suspended in a matrix substance that has a substantially larger energy bandgap, which behaves like an infinite potential barrier. Appropriate combinations of the materials that make up the colloidal QD allow us to obtain the core/shell QDs, which, when suspended in a larger bandgap matrix, present an infinite potential barrier on the surface. These single and core/shell QDs are perfectly modelable through the Konwent-like potential considering appropriate values of the A, V_0, and k parameters. Now, the smooth variation that the Konwent-like potential presents as the radial coordinate increases allows us to model the non-abrupt changes of the materials that make up the heterostructure, or even the non-abrupt changes between the dot region and the vacuum. This, in other words, allows us to model interdiffusion effects through the Konwent-like potential.

Author contributions The contributions of the authors are as follows: EBA: was responsible for numerical calculations, figures and writing of the manuscript. EK: proposed the problem and responsible for writing and editing the comments. HS: was responsible for the verification of the solution method. IS: proposed the solution method. CAD: was responsible for writing and editing the comments.

Data availibility All the files with tables, figures, and codes are available. The corresponding author will provide all the files in case they are requested.

Declarations

Conflict of interest The authors do not have any financial and non-financial competing interests statement.

Consent to Participate All co-authors participated actively in this research and agree with the final version of the manuscript.

Consent to Publish All co-authors agree with the final version of the manuscript and give their consent for it to be published, accepting all the ethical standards of the journal. The co-authors certify that this manuscript has not been published elsewhere and that it is not under consideration for publication in another journal. All relevant information has been placed in the manuscript in such a way that we guarantee the reproducibility of our research by other researchers.

References

Adachi, S.: GaAs, AlAs, and $Al_xGa_{1-x}As$: Material parameters for use in research and device applications. J. Appl. Phys. **58**, R1–R29 (1985)

Al, E.B., Kasapoglu, E., Sari, H., Sökmen, I.: Zeeman splitting, Zeeman transitions and optical absorption of an electron confined in spherical quantum dots under the magnetic field. Philos. Mag. **101**, 117–128 (2021)

Al, E.B., Kasapoglu, E., Sari, H., Sökmen, I.: Optical properties of spherical quantum dot in the presence of donor impurity under the magnetic field. Physica B **613**, 412874 (2021)

Al-Khursan, A.H., Al-Khaykanee, M.K., Al-Mossawi, K.H.: Third-order non-linear susceptibility in a three-level QD system. Photonics Nanostruc. Fundam. Appl. **7**, 153–160 (2009)

Arif, SMd., Bera, A., Ghosh, A., Ghosh, M.: Exploring noise-effect on the Intraband transition lifetime of impurity doped quantum dots. Biointerface Res. Appl. Chem. **11**, 8639–8653 (2021)

Atoyan, M.S., Kazaryan, E.M., Sarkisyan, H.: Interband light absorption in parabolic quantum dot in the presence of electrical and magnetic fields. Physica E **31**, 83–85 (2006)

Bahramiyan, H., Khordad, R.: Optical Properties of a GaAs Pyramid Quantum Dot: Second- and Third-Harmonic Generation. Int. J. Mod. Phys. B **28**, 1450053 (2014)

Barseghyan, M.G., Baghramyan, H.M., Kirakosyan, A.A., Laroze, D.: The transition from double to single quantum dot induced by THz laser field. Physica E **116**, 113758 (2020)

Beausoleil, R.G., Munro, W.J., Rodrigues, D.A., Spiller, T.P.: Applications of electromagnetically induced transparency to quantum information processing. J. Mod. Opt. **51**, 2441–2448 (2004)

Bejan, D.: Effects of electric field and structure on the electromagnetically induced transparency in double quantum dot. Opt. Mater **67**, 145–154 (2017)

Böberl, M., Kovalenko, M.V., Pillwein, G., Brunthaler, G., Heiss, W.: Quantum dot nanocolumn photodetectors for light detection in the infrared. Appl. Phys. Lett. **92**, 261113 (2008)

Çakir, B., Yakar, Y., Özmen, A.: Refractive index changes and absorption coefficients in a spherical quantum dot with parabolic potential. J. Lumin. **132**, 2659–2664 (2012)

Çakir, B., Yakar, Y., Özmen, A.: Linear and nonlinear absorption coefficients of spherical quantum dot inside external magnetic field. Physica B **510**, 86–91 (2017)

COMSOL Multiphysics, v. 5.4. COMSOL AB, Stockholm (2012a)

COMSOL Multiphysics Reference Guide, Stockholm (2012b)

COMSOL Multiphysics Users Guide, Stockholm (2012c)

Chang, W.J., Park, K.Y., Zhu, Y., Wolverton, C., Hersam, M.C., Weiss, E.A.: *n*-doping of quantum dots by lithium ion intercalation. ACS Appl. Mater. Interfaces **12**, 36523–36523 (2020)

Chiam, S.Y., Singh, R., Rockstuhl, C., Lederer, F., Zhang, W., Bettiol, A.A.: Analogue of electromagnetically induced transparency in a terahertz metamaterial. Phys. Rev. B **80**, 153103 (2009)

Clarke, J., Chen, H., van Wijngaarden, W.A.: Electromagnetically induced transparency and optical switching in a rubidium cascade system. Appl. Opt. **40**, 2047–2051 (2001)

Crnjanski, J.V., Gvozdic, D.M.: Self-consistent treatment of V-groove quantum wire band structure in nonparabolic approximation. Serb. J. Electr. Eng. **1**, 69–77 (2004)

Dahiya, S., Lahon, S., Sharma, R.: Effects of temperature and hydrostatic pressure on the optical rectification associated with the excitonic system in a semi-parabolic quantum dot. Physica E **118**, 113918 (2020)

Ducommun, Y., Kapon, E., Hohenester, U., Simserides, C., Molinari, E.: Optical spectra of single quantum dots: influence of impurities and few-particle effects. Phys. Stat. Sol. A **178**, 283–290 (2000)

Duque, C.M., Correa, J.D., Morales, A.L., Mora-Ramos, M.E., Duque, C.A.: Laterally coupled circular quantum dots under applied electric field. Physica E **77**, 34–43 (2016)

El Aouami, A., Bikerouin, M., Feddi, K., Aghoutane, N., El-Yadri, M., Feddi, E., Dujardin, F., Radu, A., Restrepo, R.L., Vinasco, J.A., Morales, A.L., Duque, C.A., Mora-Ramos, M.E.: Linear and nonlinear optical properties of a single dopant in GaN conical quantum dot with spherical cap. Philos. Mag. **100**, 2503–2523 (2020)

Elborg, Martin, Noda, Takeshi, Mano, Takaaki, Kuroda, Takashi, Yao, Yuanzhao, Sakuma, Yoshiki, Sakoda, Kazuaki: Self-assembly of vertically aligned quantum ring-dot structure by multiple droplet epitaxy. J. Cryst. Growth **477**, 239–242 (2017)

Erwin, Steven C., Lijun, Zu., Haftel, Michael I., Efros, Alexander L., Kennedy, Thomas A., Norris, David J.: Doping semiconductor nanocrystals. Nat. Lett. **436**, 91–94 (2005)

Evangelou, S.: Tailoring second-order nonlinear optical effects in coupled quantum dot-metallic nanosphere structures using the Purcell effect. Microelectron. Eng. **215**, 111019 (2019)

Fleischhauer, M., Imamoglu, A., Marangos, J.P.: Electromagnetically induced transparency: optics in coherent media. Rev. Mod. Phys. **77**, 633 (2005)

Ghajarpour-Nobandegani, S., Karimi, M.J.: Effects of hydrogenic impurity and external fields on the optical absorption in a ring-shaped elliptical quantum dot. Opt. Mater. **82**, 75–80 (2018)

El Haouari, M., Talbi, A., Feddi, E., El Ghazi, H., Oukerroum, A., Dujardin, F.: Linear and nonlinear optical properties of a single dopant in strained AlAs/GaAs spherical core/shell quantum dots. Opt. Commun. **383**, 231–237 (2017)

Harris, S.E., Yamamoto, Y.: Photon switching by quantum interference. Phys. Rev. Lett. **81**, 3611–3614 (1998)

Hau, L.V., Harris, S.E., Dutton, Z., Behroozi, C.H.: Light speed reduction to 17 metres per second in an ultracold atomic gas. Nature **397**, 594–598 (1999)

Hayrapetyan, D.B., Kazaryan, E.M., Petrosyan, L.S., Sarkisyan, H.A.: Core/shell/shell spherical quantum dot with Kratzer confining potential: impurity states and electrostatic multipoles. Physica E **66**, 7–12 (2015)

Heyn, C., Duque, C.A.: Donor impurity related optical and electronic properties of cylindrical $GaAs - Al_xGa_{1-x}As$ quantum dots under tilted electric and magnetic fields. Sci. Rep. **10**, 9155 (2020)

Heyn, Ch., Zocher, M., Pudewill, L., Runge, H., Küster, A., Hansen, W.: Droplet etched GaAs quantum dots close to surfaces and metallic interfaces. J. Appl. Phys. **121**(6), 044306 (2017)

Holovatsky, V.A., Bernik, I.B., Yakhnevych, M.. Ya..: Effect of magnetic field on energy spectrum and localization of electron in CdS/HgS/CdS/HgS/CdS multilayered spherical nanostructure. Physica B **508**, 112–117 (2017)

Holovatsky, V., Voitsekhivska, O., Bernik, I.: Effect of magnetic field on electron spectrum in spherical nano-structures. Condens. Matter. Phys. **17**, 13702 (2014)

Holovatsky, V.A., Voitsekhivska, O.M., Ya Yakhnevych, M.: The effect of magnetic field and donor impurity on electron spectrum in spherical core-shell quantum dot. Superlattice Microst. **116**, 9–16 (2018)

Holovatsky, V.A., Voitsekhivska, O.M., Yakhnevych, M.. Ya..: Effect of magnetic field on an electronic structure and intraband quantum transitions in multishell quantum dots. Physica E **93**, 295–300 (2017)

Horiguchi, Naoto, Futatsugi, Toshiro, Nakata, Yoshiaki, Yokoyama, Naoki, Mankad, Tanaya, Petroff, Pierre M.: Quantum dot infrared photodetector using modulation doped InAs self-assembled quantum dots. Jpn. J. Appl. Phys. **38**, 2559–2561 (1999)

Hosseinpour, P., Soltani-Vala, A., Barvestani, J.: Effect of impurity on the absorption of a parabolic quantum dot with including Rashba spin-orbit interaction. Physica E **80**, 48–52 (2016)

Karabulut, I., Baskoutas, S.: Second and third harmonic generation susceptibilities of spherical quantum dots: effects of impurities, electric field and size. J. Comput. Theor. Nanosci. **6**, 153–156 (2009)

Karaca Boz, F., Nisanci, B., Aktas, S., Okan, S.E.: Energy levels of GaAs/AlxGa1-xAs/AlAs spherical uantum dot with an impurity. Appl. Surf. Sci. **387**, 76–81 (2016)

Kasapoglu, E., Ungan, F., Sari, H., Sökmen, I., Mora-Ramos, M.E., Duque, C.A.: Donor impurity states and related optical responses in triangular quantum dots under applied electric field. Superlattice Microst. **73**, 171–184 (2014)

Khordad, R., Bahramiyan, H.: The second and third-harmonic generation of modified Gaussian quantum dots under influence of polaron effects. Superlattice Microst. **76**, 163–173 (2014)

Khordad, R., Bahramiyan, H., Mohammadi, S.A.: Influence of impurity on binding energy and optical properties of lens shaped quantum dots: Finite element method and Arnoldi algorithm. Chin. J. Phys. **54**, 20–32 (2016)

Kilic, D.G., Sakiroglu, S., Kasapoglu, E., Sari, H., Sökmen, I.: Impurity-modulated optical response of a disc-shaped quantum dot subjected to laser radiation. Photon. Nanostruct. **38**, 100748 (2020)

Konwent, H.: One-dimensional Schrödinger equation with a new type double-well potential. Phys. Lett. A **118**, 467–470 (1986)

Kria, M., El-Yadri, M., Aghoutane, N., Pérez, L.M., Laroze, D., Feddi, E.: Forecasting and analysis of nonlinear optical responses by tuning the thickness of a doped hollow cylindrical quantum dot. Chin. J. Phys. **66**, 444–452 (2020)

Laroze, D., Barseghyan, M., Radu, A., Kirakosyan, A.A.: Laser driven impurity states in two-dimensional quantum dots and quantum rings. Physica B **501**, 1–4 (2016)

Li, K., Guo, K., Liang, L.: Effect of the shape of quantum dots on the refractive index changes. Physica B **502**, 146–150 (2016)

Lu, L., Xie, W., Hassanabadi, H.: The effects of intense laser on nonlinear properties of shallow donor impurities in quantum dots with the Woods-Saxon potential. J. Lumin. **131**, 2538–2543 (2011)

Ma, S.M., Xu, H., Ham, B.S.: Electromagnetically-induced transparency and slow light in GaAs/AlGaAs multiple quantum wells in a transient regime. Opt. Express **17**, 14902–14908 (2009)

Makhlouf, D., Choubani, M., Saidi, F., Maaref, H.: Applied electric and magnetic fields effects on the nonlinear optical rectification and the carrier's transition lifetime in InAs/GaAs core/shell quantum dot. Mater. Chem. Phys. **267**, 124660 (2021)

Makkar, Mahima, Viswanatha, Ranjani: Frontier challenges in doping quantum dots: synthesis and characterization. RSC Adv. **8**, 22103–22112 (2018)

Marangos, J.P., Halfmann, T.: *Handbook of Optics*, edited by M. Bass, 3rd edn. Vol. 4, New York: McGraw-Hill, **14**(1), (2009)

McDonald, S.A., Cyr, P.W., Levina, L., Sargent, E.H.: Photoconductivity from PbS-nanocrystal/semiconducting polymer composites for solution-processible, quantum-size tunable infrared photodetectors. Appl. Phys. Lett. **85**, 2089 (2004)

Mora-Ramos, M.E., El Aouami, A., Feddi, E., Radu, A., Restrepo, R.L., Vinasco, J.A., Morales, A.L., Duque, C.A.: Donor impurity energy and optical absorption in spherical sector quantum dots. Heliyon **6**, e03194 (2020)

Mora-Ramos, M.E., Vinasco, J.A., Laroze, D., Radu, A., Restrepo, R.L., Heyn, C., Tulupenko, V., Hieu, N.N., Phuc, H.V., Ojeda, J.H., Morales, A.L., Duque, C.A.: Electronic structure of vertically coupled quantum dot-ring heterostructures under applied electromagnetic probes. A finite-element approach. Sci. Rep. **11**(16), 4015 (2021)

Máthé, L., Onyenegecha, C.P., Farcaş, A.-A., Pioraş-Ţimbolmaş, L.-M., Solaimani, M., Hassanabadi, H.: Linear and nonlinear optical properties in spherical quantum dots: inversely quadratic Hellmann potential. Phys. Lett. **397**, 127262 (2021)

Niculescu, E.C., Bejan, D.: Nonlinear optical properties of GaAs pyramidal quantum dots: effects of elliptically polarized radiation, impurity, and magnetic applied fields. Physica E **74**, 51–58 (2015)

Niculescu, E.C., Stan, C., Cristea, M., Truscă, C.R.: Magnetic-field dependence of the impurity states in a dome-shaped quantum dot. Chem. Phys. **493**, 32–41 (2017)

Papagiorgis, P., Stavrinadis, A., Othonos, A., Konstantatos, G., Itskos, G.: The influence of doping on the optoelectronic properties of PbS colloidal quantum dot solids. Sci. Rep. **6**, 18735 (2016)

Pulgar-Velásquez, L., Sierra-Ortega, J., Vinasco, J.A., Laroze, D., Radu, A., Kasapoglu, E., Restrepo, R.L., Gil-Corrales, J.A., Morales, A.L., Duque, C.A.: Shallow donor impurity states with excitonic contribution in GaAs/AlGaAs and CdTe/CdSe truncated conical quantum dots under applied magnetic field. Nanomaterials **11**(13), 2832 (2021)

Radu, C., Radu, A., Vinasco, J.A., Laroze, D., Restrepo, R.L., Tulupenko, V., Hieu, N.N., Phuc, H.V., Mora-Ramos, M.E., Ojeda, J.H., Morales, A.L., Duque, C.A.: Exciton states in conical quantum dots under applied electric and magnetic fields. Opt. Laser Technol. **139**(13), 106953 (2021)

Rahimi, F., Ghaffary, T., Naimi, Y., Khajehazad, H.: Effect of magnetic field on energy states and optical properties of quantum dots and quantum antidots. Opt. Quant. Electron. **53**, 47–62 (2021)

Rahul, K.S., Devaraj, N., Babu, R.K., Mathew, S., Salini, K., Mathew, V.: Intraband absorption of D^- center in CdSe/CdS/CdSe/CdS multilayer quantum dot. J. Phys. Chem. Solid. **106**, 99–104 (2017)

Rezaei, G., Kish, S.S.: Linear and nonlinear optical properties of a hydrogenic impurity confined in a two-dimensional quantum dot: effects of hydrostatic pressure, external electric and magnetic fields. Superlattice Microst. **53**, 99–112 (2013)

Sadeghi, E., Naghdi, E.: Effect of electric and magnetic fields on impurity binding energy in zinc-blend symmetric InGaN/GaN multiple quantum dots. Nano Converg. **1**, 25 (2014)

Safarpour, Gh., Izadi, M.A., Novzari, M., Niknam, E.: External electric field effect on the nonlinear optical properties of a laser dressed donor impurity in a $GaAs$ spherical quantum dot confined at the center of a $Ga_{1-x}Al_xAs$ cylindrical nano-wire. Indian J. Pure Appl. Phys. **53**, 247–256 (2015)

Sargsian, T.A., Mkrtchyan, M.A., Sarkisyan, H.A., Hayrapetyan, D.B.: Effects of external electric and magnetic fields on the linear and nonlinear optical properties of InAs cylindrical quantum dot with modified Pöschl-Teller and Morse confinement potentials. Physica E **126**, 114440 (2021)

Sari, H., Kasapoglu, E., Sakiroglu, S., Sökmen, I., Duque, C.A.: Impurity-related optical response in a 2D and 3D quantum dot with Gaussian confinement under intense laser field. Philos. Mag. **100**, 619–641 (2020)

Segal, D., Nitzan, A.: Thermal conductance through molecular wires. J. Chem. Phys. **119**, 6840 (2003)

Sharma, H.K., Boda, A., Boyacioglu, B., Chatterjee, A.: Electronic and magnetic properties of a two-electron Gaussian GaAs quantum dot with spin-Zeeman term: a study by numerical diagonalization. J. Magn. Magn. Mater. **469**, 171–177 (2019)

Shi, L., Yan, Z.W.: Linear and nonlinear optical properties of an off-center donor in GaAs/AlGaAs and AlGaAs/GaAs core-shell ellipsoidal quantum dots. Superlattice Microst. **109**, 382–393 (2017)

Stevanović, L., Filipović, N., Pavlović, V.: Effect of magnetic field on absorption coefficients, refractive index changes and group index of spherical quantum dot with hydrogenic impurity. Opt. Mater. **91**, 62–69 (2019)

Sugawara, M., Hatori, N., Ebe, H., Ishida, M., Arakawa, Y., Akiyama, T., Otsubo, K., Nakata, Y.: Modeling room-temperature lasing spectra of 1.3-μ m self-assembled InAs/GaAs quantum-dot lasers: Homogeneous broadening of optical gain under current injection. J. Appl. Phys. **97**, 043523 (2005)

Talbi, A., El Haouari, M., Nouneh, K., Pérez, L.M., Tiutiunnyk, A., Laroze, D., Courel, M., Mora-Ramos, M.E., Feddi, E.: LO-Phonons and dielectric polarization effects on the electronic properties of doped GaN/InN spherical core/shell quantum dots in a nonparabolic band model. Appl. Phys. A **127**, 1–17 (2021)

Tiutiunnyk, A., Tulupenko, V., Mora-Ramos, M.E., Kasapoglu, E., Ungan, F., Sari, H., Sökmen, I., Duque, C.A.: Electron-related optical responses in triangular quantum dots. Physica E **60**, 127–132 (2014)

Vahdani, M.R.K.: The effect of the electronic intersubband transitions of quantum dots on the linear and nonlinear optical properties of dot-matrix system. Superlattice Microst. **76**, 326–338 (2014)

Varshni, Y.P.: Effect of an intense laser field on donor impurities in spherical quantum dots. Superlattice. Microst. **30**, 45–52 (2001)

Xu, Q., Sandhu, S., Povinelli, M.L., Shakya, J., Fan, S., Lipson, M.: Experimental realization of an on-chip all-optical analogue to electromagnetically induced transparency. Phys. Rev. Lett. **96**, 123901 (2006)

Zhang, Z.H., Guo, K.X., Chen, B., Wang, R.Z., Kang, M.W., Shao, S.: Theoretical studies on the optical absorption coefficients and refractive index changes in parabolic quantum dots in the presence of electric and magnetic fields. Superlattice Microst. **47**, 325–334 (2010)

Zhang, Hui, Liu, Jiabin, Wang, Chao, Selopal, Gurpreet S., Barba, David, Wang, Zhiming M., Sun, Shuhui, Zhao, Haiguang, Rosei, Federico: Near-infrared colloidal manganese doped quantum dots: photoluminescence mechanism and temperature response. ACS Photonics **6**, 2421–2431 (2019)

Zhang, S., Zhou, S., Loy, M.M.T., Wong, G.K.L., Du, S.: Optical storage with electromagnetically induced transparency in a dense cold atomic ensemble. Opt. Lett. **36**, 4530–4532 (2011)